Energy 263 (2023) 125382

Contents lists available at ScienceDirect

Energy

journal homepage: www.elsevier.com/locate/energy

Thermal performance assessment and control optimization of a solar-driven seasonal sorption storage system for residential application

Alicia Crespo [a,*], Cèsar Fernández [a], David Vérez [a], Joan Tarragona [a], Emiliano Borri [a], Andrea Frazzica [b], Luisa F. Cabeza [a], Alvaro de Gracia [a]

[a] GREiA Research Group, Universitat de Lleida, Pere de Cabrera s/n, 25001 Lleida, Spain
[b] Institito di Tecnologie Avanzate per l'Energia "Nicola Giordano",CNR-ITAE, Messina, Italy

ARTICLE INFO

Keywords:
Seasonal thermal energy storage
Control optimization
Numerical simulation
Sorbent water materials
Sorption storage

ABSTRACT

The present paper analyzed the thermal performance and control optimization of a solar system based on seasonal sorption storage for domestic applications. The system control, which could choose between 41 operational modes, was optimized based on operational costs and maximization of sorption system use. The system was composed by 17.5 m^2 of evacuated tube collectors, 3.6 m^3 of composite sorbents based on lithium chloride and a stratified water tank. High efficiency of a sorption storage system was obtained when continuous charges or discharges occur, which, in this study, depended on weather conditions (ambient temperature and solar irradiation). The operational economic benefits were maximized using a sorption system with 9% less capacity and, therefore, less storage volume. The sorption thermal energy storage system obtained energy densities of 90 and 106 kWh/m^3. The whole system could supply 35% of the total thermal demand of a single family house in Nuremberg. The study concluded that the control optimization of a seasonal sorption system is a key factor to make the technology competitive, define its optimal size and, therefore, maximize its energy density in further designs.

1. Introduction

The building sector consumes around one-third of the worldwide total final energy [1]. Energy consumption for domestic hot water (DHW) and space heating (SH) achieves a high percentage (14.8% and 63.6%, respectively) of the total energy consumption of a EU household [2]. Solar thermal systems are a good solution to supply the thermal energy demand of buildings, allowing CO_2 savings. Especially, in climates such as middle and north Europe, the temporal mismatch between high solar irradiation during summer and high space heating demand during winter justifies the need of seasonal thermal energy storage (STES). Thermal energy storage (TES) based on sorption technology can store heat with low thermal losses during the idle period, which makes it very attractive for STES. Furthermore, thermochemical sorption technology has been recognized as one of the most promising technologies for STES due to the large storage density and its less influence on ambient temperature compared to sensible or latent heat storage technologies [3].

Different authors already studied experimentally sorption TES systems for domestic applications [4–8]. Nevertheless, the integration of these systems into a whole building heating energy system needs a detailed study of its performance, in particular, when its performance depends on weather conditions (i.e., solar energy as heat source) and transient thermal demands. The performance analysis and optimization of a seasonal sorption system integrated into a building can be performed through numerical simulations. For example, Engel et al. [9] presented the simulation of a validated sorption heating system for different locations in Europe using zeolite as storage material. Due to its modularity, the system could choose between 30 operational modes. Nevertheless, the control settings were not optimal for every scenario. The authors highlighted the beneficial effect of the "charge boost" mode, which enabled vapor transfer between two sorption stores of different temperature level and/or state of charge. Ma et al. [10] assessed the potential of seasonal solar TES system using ammonia-based chemisorption with application in UK dwellings. The best case scenario could covered 57.4% of the total SH demand using 45 m^3 of $BaCl_2$-0/8NH_3 STES. Tzinnis et al. [11] studied the building integration of a liquid sorption storage combined with an air-source electric heat pump driven by solar photovoltaic panels. Winter electricity demand and emission reductions reached values up to 41%. Mlakar et al. [12] showed the advantages of thermochemical storage compared to sensible heat storage to provide energy demand coverage

* Corresponding author.
E-mail address: alvaro.degracia@udl.cat (A. Crespo).

https://doi.org/10.1016/j.energy.2022.125382
Received 16 January 2022; Received in revised form 11 July 2022; Accepted 4 September 2022
Available online 30 September 2022

Nomenclature

Symbols

Q	Thermal power [kW]
$\dot{m}$	Mass flow rate [kg/s]
A_{col}	Area of collector [m^2]
E_G	Titled global solar irradiation [W/m^2]
E_d	Beam solar irradiation [W/m^2]
E_{diff}	Diffuse solar irradiation [W/m^2]
T	Temperature [°C]
$T_{aver,coll}$	Collector's average temperature [°C]
$U_{L,col}$	Collector's heat losses transfer coefficient [W/m^2 K]
$\eta_{overall}$	Overall collector efficiency
F_r	Heat removal factor
a_0	Collector's optical efficiency
a_1	First order collector efficiency [W/m^2 K]
a_2	Second order collector efficiency [W/m^2 K^2]
IAM	Incidence angle modifier of collector
E	Thermal energy [kWh]
C_p	Specific heat [J/kg K]
J	Last time-step
t	Time
C	Unitary cost [€/kWh]
e_d	Energy density [kWh/m^3]
D	Thermal demand [kWh]
V	Volume [m^3]
u	Uncertainty [%]

Acronyms

DHW	Domestic hot water
SH	Space heating
STES	Seasonal thermal energy storage
TES	Thermal energy storage
PCM	Phase change materials
COP	Coefficient of performance
RBC	Rule based control
HTF	Heat transfer fluid
SF	Solar fraction

Subscripts

coll	Collector
set	Setpoint
sens	Sensible
amb	Ambient
in	Inlet
out	Outlet
des	Desorption
ads	Adsorption
evap	Evaporator of sorption storage system
cond	Condenser of sorption storage system
sorb	Sorbent material
wt	Water tank
s	Summer
w	Winter
min	Minimum
max	Maximum
cl	Close loop
b	Boiler
el	Electrical
nosup	Not supplied demand

for a building in Slovenia. The software TRNSYS was used to simulate the system a macro scale. Thinsurat et al. [13] analyzed the potential of an hybrid solar photovoltaic-thermal (PV/T) collector coupled to a thermo-chemical sorption TES system. It was found that a 26 m^2 air gap PV/T collector coupled to the sorption storage could fully satisfy the annual hot water demand of a single household in Newcastle with 100% solar sources.

Some studies integrated new components or operational modes in the system to improve the sorption storage system performance, especially during its discharge on cold winter days. For instance, Ma et al. [14] studied a solar driven seasonal thermochemical sorption system assisted with an electric heater or an electric-driven compressor to supplement the thermochemical desorption process when there was not enough solar irradiation. Those authors concluded that the compressor substantially improved the heat storage capacity in comparison with the use of the electric heater. Jiang et al. [15] studied the performance of a sorption seasonal TES assisted by a compressor under ultra-low ambient temperatures. The authors concluded that the hybrid sorption TES driven by a photovoltaic-thermal system was promising for severe cold regions. In a different study, Jiang at el. [16] analyzed an hybrid compression-assisted sorption thermal battery for thermal storage. The results indicated good system compactness for real application. Li et al. [3] analyzed an innovative dual-mode sorption system for seasonal storage. The system achieved a COP of 0.6 and an energy density above 1000 kJ/kg. The authors highlighted the advantages of the sorption system over sensible and latent heat storage.

Scapino et al. [17] presented a techno-economical optimization of a geothermal energy system with sorption TES that supplied heat to an ORC and to a district heating system. The optimization aimed at finding the optimal STES size and system operational behavior under different energy markets. Bau et al. [18] optimized the design of an adsorber-bed for its application on chillers. To ensure that intrinsic design properties are not affected by a poor control, a control optimization was also studied. The goal of the authors was to define a method to efficiently design adsorbed-beds. Frazzica et al. [19] proposed a unified methodology for the evaluation of the potential of seasonal sorption storage based on building constraints, weather conditions and solar thermal technology. The results demonstrated that the STES density varies significantly with the SH demand and the ambient heat source/sink. Nevertheless, as the authors highlighted, a pure dynamic modeling to evaluate the dynamic behavior of the system was missing in the study.

The integration of solar collectors coupled to a seasonal sorption system is a good solution to substitute fossil fuels for supplying households heat needs. Nevertheless, as Frazzica et al. [19] reported, a carefully preliminary analysis to avoid overestimation of the STES volume is necessary. Indeed, sorption storage system must operate at its maximum efficiency to be competitive against traditional fossil fuels, since their operation is more complicated. As previously reviewed, several studies have reported an upgrade of the sorption storage or have optimized its size from a technical and/or economic perspective showing promising results. However, in spite of the potential of sorption technology as seasonal storage, its dependency on weather conditions (ambient temperature and solar irradiation) can limit its operation and therefore its energy density if a proper operation is not explored. Moreover, as N'Tsoukpoe et al. [20] reported, seasonal sorption storage systems are subjected to significant sensible thermal losses. A control optimization

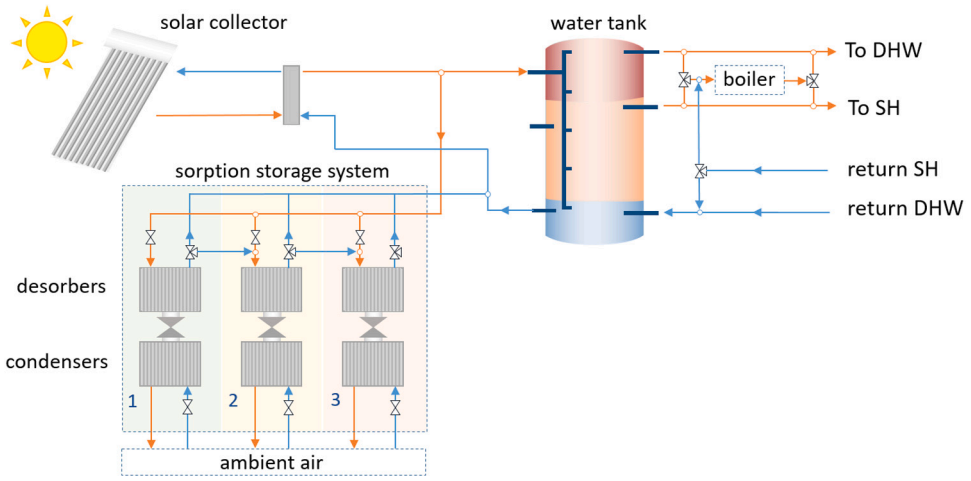

Fig. 1. Schematic of the system for summer operating conditions (charging STES mode).

based on weather conditions, system state and thermal demand allows to minimize the sensible thermal losses and maximize its efficiency.

This study goals to analyze the impact of a detailed control optimization on the performance and thermal losses of a water-based seasonal sorption system driven by solar energy. For this purpose, a detailed control optimization of a solar driven sorption storage system, which provides thermal demand to a single-family house in middle Europe, was performed for first time in the found literature. This system was developed within the frame of the EU-Horizon 2020 SWS-Heating project. In the project, a novel composite water sorbent material — employing silica gel as matrix and lithium chloride as active embedded salt [21] was developed to be used in a sorption storage. It was based on an innovative modular architecture, employing highly asymmetric plate heat exchangers as adsorbers [22], in which the loose grains of the composite sorbent are embedded. The system was controlled using a rule based control (RBC) strategy, which consists of a control policy where a set of rules govern the behavior of the system.

This study is organized as follows: in Section 2 a description of the system and its operation is reported. In Section 3, the methodology is presented. In Section 4, the results for the two optimized scenarios are presented and discussed. Section 5 includes the conclusions and future work.

2. Description of the system

In this study a solar energy system based on a seasonal sorption TES, latent heat storage and a stratified water tank able to supply heating energy for SH and DHW is presented. A schematic of the system for the two studied operating conditions, summer and winter, is shown in Figs. 1 and 2. In summer, at high solar irradiation conditions, the sorption modules were charged with solar heat at around 90 °C, while part of the solar energy (at 70 °C) was provided to the combi-tank and used to provide the needed DHW. The heating energy, provided at the desorption temperature requested by the composite sorbent, caused the desorption of the water vapor adsorbed onto the composite sorbent. The water vapor leaving the composite was condensed rejecting the condensation heat to the ambient.

In winter, when SH was required by the user in the next 24 h and the water tank temperature fell below the setpoint temperature, the sorption modules were activated and discharged, providing energy to the water tank. For this purpose, the water was evaporated again, using a low temperature heat source (at temperature from 5 to 15 °C), and it was adsorbed by the sorbent material. Heat of sorption was then released from the reactor to the water tank (at around 35 °C) to supply the SH demand. Most of the sorption systems [3,9,10,23–25] used, ambient air as low temperature heat source, which causes great system dependency on the ambient temperature and limitations in its operational, especially, during cold winter days when water is employed as working fluid. In the proposed system in order to reduce the system dependency on ambient temperature, the solar thermal field was exploited in winter, when the irradiation is low, to provide the low temperature heat source to the STES evaporator. Furthermore, a tank filled with phase change material (PCM) [26] able to provide heat at a nearly constant temperature (melting temperature: 15 °C), was included, in order to store at high energy density the heating energy provided by the solar field, thus extending the operation of the STES. Specifically, in winter, whenever the PCM tank was not fully charged and the solar field could provide the required energy, it was directly charged at low temperature (20 °C) by the solar field. The system allowed the simultaneous charge of the PCM with solar heat and its discharge to assist the evaporator of the sorption modules.

The solar field could also provide heat to the water tank along the year for DHW or SH at a collector outlet temperature setpoint of 70 or 45 °C (a temperature difference in the heat exchanger should be considered), respectively. Furthermore, the system was assisted by a back-up gas boiler in case the water tank was not at the DHW or SH setpoint temperatures. When the temperature in the water tank fell well below the SH setpoint temperature, the SH circuit operated in a close loop with the boiler. In winter, in case the boiler had a simultaneous demand of both SH and DHW, DHW was prioritized. Radiant floor was selected as the SH distribution system of the house. The adsorption temperature (and sorbent composite) was set considering the usual required temperatures in floor heating. The authors considered constant SH supply and return temperature of 38 and 28 °C.

The seasonal solar-driven heating system could operate with one of the 41 operational modes, presented in Annex, which are the combination of the different operational modes of the subcomponents described in the previous paragraphs. The operational modes of the solar collectors and, consequently, of the whole system, were selected based on the instantaneous solar irradiation availability. Four thresholds of solar irradiation were set to define the control strategy, whose values had great impact on the sorption system performance and efficiency. Therefore, in this study, the optimization of the RBC strategy of a solar driven seasonal system based on a sorption storage tank was performed. The methodology considered for that purpose is explained in the following section.

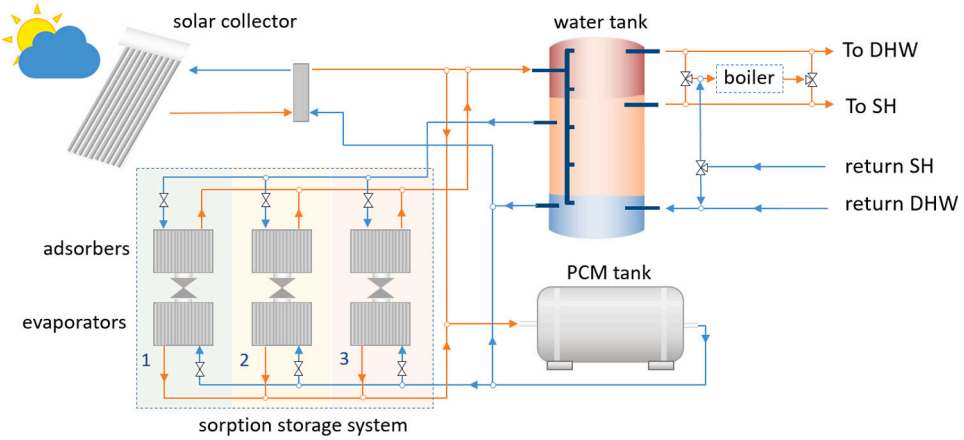

Fig. 2. Schematic of the system for winter operating conditions (discharging STES mode).

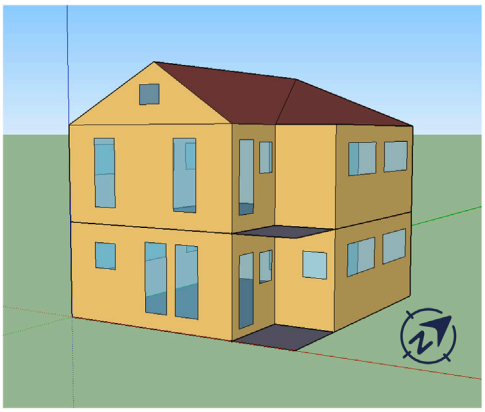

Fig. 3. Sketch of the designed and simulated building.

3. Methodology

3.1. Input data: thermal demands and weather data

To obtain the SH consumption profiles employed in this study, a building model was designed using the OpenStudio software [27] and simulated through EnergyPlus [28]. The building and its wall thermal transmittance values were defined using the Tabula/Episcope Database [29] for the reference building with code: DE.N.SFH.12.Gen considering a single family house (code:EFH_L). A building sketch can be seen in Fig. 3. The total SH demand of the building was calculated for two floors with a surface of 67 m^2 each (the attic zone was not conditioned). To have a better understanding of the heating set points employed in each area, Fig. 4 details the thermostat operation considered in the living and the sleeping areas, which correspond to a low demand consumer. Indeed, these modest space heating demands were obtained from a technical report [30] and correspond to a near zero emissions building (NZEB). The data was generated with a time-step of one hour.

Regarding the DHW, a consumption of 90 l/day [30] with a temperature rise from 10 to 60 °C was considered. DHW data was firstly obtained hourly-based, and interpolated to the first 15 min of every hour to simulate daily activities that consume DHW: shower, wash dishes, etc.

Meteorological data [31] of different years for the location of Nuremberg was considered to run both the simulations of the building in EnergyPlus and the simulations of the energy system in Python.

3.2. Description of the physical models

Physical models of every subcomponent were necessary to assess the thermal performance of the system and optimize its control. All physical models were implemented in Python 3 [32] and are described in detail in the following subsections.

3.2.1. Evacuated tube collectors

The energy balance equation of an evacuated tube collector, presented by Duffie and Beckmann [33], can be expressed based on the overall collector efficiency ($\eta_{overall}$), as described in (1).

$$IAM \cdot E_G \cdot A_{col} \cdot \eta_{overall} = \dot{m}_{col} \cdot C_p \cdot (T_{out,col} - T_{in,col}) \quad (1)$$

The overall collector efficiency can be described as:

$$\eta_{overall} = a0 - a1 \cdot \frac{T_{aver} - T_{amb}}{E_G} - a2 \cdot \frac{(T_{aver} - T_{amb})^2}{E_G} \quad (2)$$

The model of the solar collector was validated using the results of the collector outlet temperatures presented by Ayompe et al. [34]. The collector outlet temperature of both: the reference paper and the numerical results of the present study, are shown in Fig. 5. The model presents an average relative error lower than 1% in predicting the collector outlet temperature.

The heat transfer between the solar field and the secondary loop was done through a heat exchanger simulated using the traditional epsilon-NTU method [35].

3.2.2. Sorption modules

To reduce the computational time of the whole system simulation, the sorption modules were simulated using a performance map approach, which is computationally lighter than a physical model. In particular, the performance maps in terms of charging and discharging power as a function of inlet temperatures at the main components of the STES were obtained scaling up the results reported on the characterization of a lab-scale adsorber configuration reported in Mikhaeil et al. [22]. It consisted of an asymmetric plate heat exchanger filled with the composite sorbent material. The lab-scale testing performed by Brancato et al. [36] to define the kinetics of the water sorbent composite together with the adsorber characterization performed by Mikhaeil et al. [22] were exploited to define the adsorption/desorption kinetic of the process, scaled-up to draw the performance maps reported in Fig. 6, which were calculated considering a modular system using adsorbers containing 100 kg of composite sorbent employing silica gel impregnated with 30 wt% of LiCl and considering the following constant mass flow rates: 0.2 kg/s for the absorber and desorber, 0.166 kg/s for the evaporator and 0.25 kg/s for the condenser. As can be argued, during charging phase, the desorption power increases with

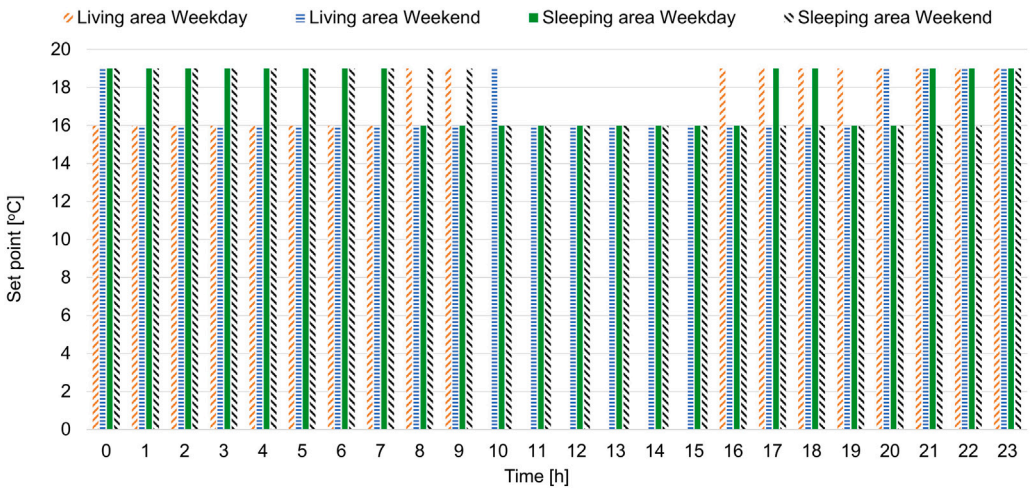

Fig. 4. Temperature setpoints for the space heating.

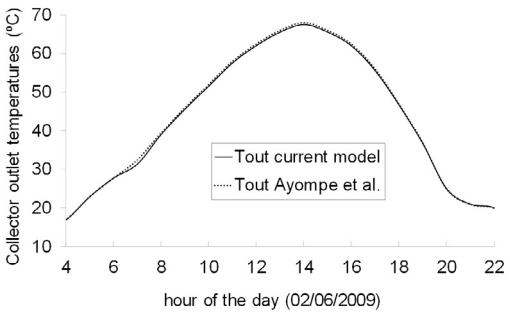

Fig. 5. Comparison between numerical results of the current model and literature results (Ayompe et al. [34]) based on collector outlet temperature.

increasing the inlet temperature at the adsorber reactors and decreasing the inlet temperature at the condenser. This behavior is justified by the increasing kinetic of the process achieved at high temperature and the higher water vapor exchanged when the condensation temperature is reduced. Similar considerations can be reported looking at the discharging phase. Indeed, in this case, the kinetic increases with increasing the evaporation pressure, while the water vapor exchanged increases when the adsorption temperature is reduced. The simulated configuration, according to the equilibrium thermodynamic curves reported in [21], can store up to 110 MJ of energy per module.

The desorption heat power (Q_{des}) was obtained based on the condenser inlet temperature – ambient temperature – and the desorber inlet temperature using Fig. 6(a). In the same way (using Fig. 6(b)), the adsorption heat power (Q_{ads}) was obtained based on the evaporator inlet temperature and the adsorber inlet temperature. Using those values and Eqs. (3) and (4), (5), (6), the outlet desorption and condenser temperature, as well as the outlet adsorption and evaporator temperature in the module were calculated. Specifically, in evaluating evaporation and condensation power, as reported in Eqs. (5) and (6), the average ratio between adsorption enthalpy and water condensation/evaporation enthalpy was considered, which equals to 1.2.

Furthermore, in order to properly consider the operational constraints of a STES, also the sensible losses were considered. Indeed, during the stand-by periods between two consecutive charging or discharging phases, the STES is subjected to heat losses to the surrounding, which reduce the temperature of the whole module, comprising metal, water and composite sorbent. For the sake of simplicity, the STES was assumed as a lumped system, in which a single temperature can be used to represent the cooling down due to the heat losses. Accordingly, the temperature evolution was obtained considering the STES geometrical features, as well as the mass of composite sorbent loaded and a standard polyurethane insulation (5 cm thick). The heat losses were calculated considering natural convection towards the surrounding ambient, using an average ambient temperature of 15 and 21 °C for winter and summer, respectively. Under these conditions, the temperature decrease of the STES can be described by an exponential decay function, depending on the natural convection coefficient, the external surface area and the thermal mass of the STES [37]. Of course, any temperature decrease of the STES during the stand-by periods is associated with a energy loss that must be provided during the following phase in order to either increase the STES temperature at the minimum desorption temperature (charging phase) or to increase the STES temperature at the adsorption temperature needed to deliver heat to the user (discharging phase). The energy will be then extracted from the solar field in the former case and will be part of the adsorption heat released by the adsorbent material in the latter case. Clearly, the longer the stand-by the higher the overall heat losses. Fig. 7 summarizes the obtained results during both, charging and discharging periods, where for a certain sorbent temperature of the module (T_{sorb}) the required sensible energy ($E_{req,sens}$) to reach the adsorption or desorption temperature is given. As expected, since the temperature difference is much higher between charging and ambient temperature, the phase which is mainly affected by the heat losses is the charging one.

Accordingly, this effect must be carefully taken into account when the optimal control strategy is investigated, since it can strongly affect the decision making process.

$$Q_{des} = \dot{m}_{des} \cdot C_p \cdot (T_{out,des} - T_{in,des}) \tag{3}$$

$$Q_{ads} = \dot{m}_{ads} \cdot C_p \cdot (T_{out,ads} - T_{in,ads}) \tag{4}$$

$$Q_{evap} = \frac{Q_{des}}{1.2} = \dot{m}_{evap} \cdot C_p \cdot (T_{in,evap} - T_{out,evap}) \tag{5}$$

$$Q_{cond} = \frac{Q_{ads}}{1.2} = \dot{m}_{cond} \cdot C_p \cdot (T_{out,cond} - T_{in,cond}) \tag{6}$$

3.2.3. PCM tank

The PCM tank consisted of a rectangular tank filled with horizontal PCM slabs stacked with a gap between them to allow the flow of the heat transfer fluid (HTF). The PCM tank used in this study was described in detail in a previous work presented by Crespo et al. [38]. In that study, a 2D numerical model based on finite control volume

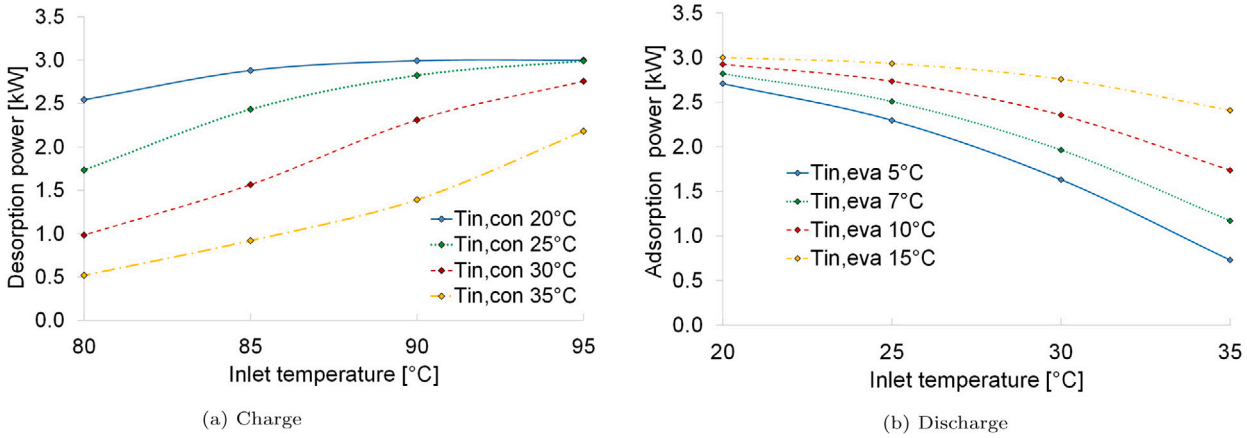

(a) Charge (b) Discharge

Fig. 6. Performance map for the charging and discharging power of the sorption module.

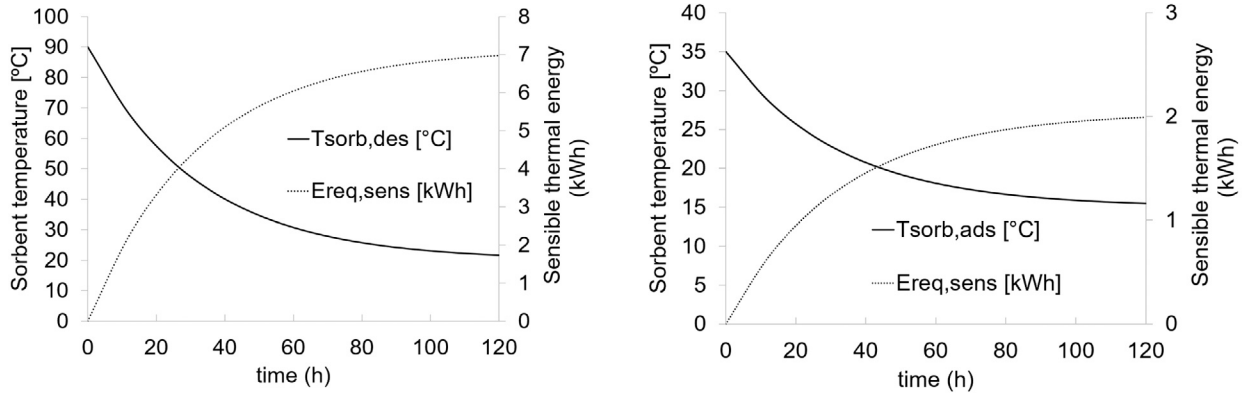

(a) Charge (b) Discharge

Fig. 7. Temperature evolution and sensible energy associated to the STES heat losses towards the environment for both charging and discharging periods.

method was developed and validated to evaluate the thermal performance of the PCM tank. The 2D model considered nodes in the x-axis (N_x), HTF direction, and in the y-axis, in both PCM (N_{pcm}) and slab wall (N_{wall}). In the present study, to reduce the computational time, the combination $N_x = 10$, $N_{pcm} = 7$, $N_{wall} = 3$ was considered. This combination reduced the computational effort in 25% (compared to the reference) and obtained a average relative error of the results of 4%.

3.2.4. Stratified water tank

The water tank of the system consisted of a constant volume stratified water tank. A 1D numerical model based on finite control volume method was developed to analyze its performance. Each control volume was fully mixed and an explicit scheme was used to solve the energy balance equations. The physical phenomena considered in the 1D model was: thermal losses to the ambient, conduction between nodes and mass flow between nodes. Buoyancy effect was neglected. Thermal instabilities between adjacent nodes due to the non consideration of the buoyancy effect were solved by temperature node mixing [39]. The equations used to simulate the heat transfer in a 1D stratified water tank model were presented by Rodriguez-Hidalgo et al. [40].

Experiments to validate the model were carried out at the laboratory of the GREiA research group at the University of Lleida (Spain). The experimental set-up, consisted of a stratified water tank of 535 liters with a vacuum insulated double wall with five sensors located along the tank (see Fig. 8). The experiment used for validation consisted in a charge process with water inlet at the top node at 45 °C (T1 — see Fig. 8) and water outlet from the bottom node (T5 — see Fig. 8. The initial temperature of the tank was 25.3 °C. A constant mass flow rate of 3.33 l/min was considered in the test. More information about the experimental set-up can be found in Verez et al. [41]. The thermal and physical tank parameters are shown in Table 1.

The water tank did not have a perfect cylindrical shape as shown in Fig. 8. To facilitate its modeling, a perfect cylindrical shape with an equivalent height of 1.65 m was considered. In this study, due to the tank geometry and the sensors position, and to reach a trade-off between results accuracy and computational time, 33 nodes were selected to compare the computational results with the experiments. The comparison between tank outlet temperature of the experiment and the numerical model are shown in Fig. 9. The average relative error of the five sensors was calculated for the values with experimental temperatures higher than 25.5 °C. The errors were: 0.6% for T1, 2.1% for T2, 1.9% for T3, 2.3% for T4 and 3.8% for T5. The highest deviation occurred at the bottom part of the water tank. Nevertheless, to reach a trade-off between results accuracy and computational time, the model using 33 nodes was considered accurate enough for the purpose of this study.

Furthermore, to ensure accuracy of the reported results, an uncertainty analysis to the heat transfer rate ($u(\dot{Q})$) was carried out according to the GUM methodology [43], a methodology exemplified in [44]. To calculate the uncertainty of the heat transfer rate delivered by the stratified water tank, the uncertainty from the different involved variables was taken into account: 0.0002% [45] for the HTF density, 0.3% (given by the manufacturer) for the volumetric flow rate, 1.5% [46] for the specific heat capacity and an accuracy of $\pm 0.15+0.002\ T$ of Pt-100 class A temperature sensors [47]. Based on this data, using Eq. (7) a relative expanded uncertainty (k = 2) for the heat transfer rate of 3.3% was

Table 1
Parameters of the water tank used to validate the 1D model.

Parameter	Value	Parameter	Value
Top heat losses coefficient (W/m^2 K)	0.32 [41]	Tank volume (l)	1000
Edges heat losses coefficient (W/m^2 K)	0.38 [41]	Equivalent tank height (m)	1.65
Bottom heat losses coefficient (W/m^2 K)	2 [41]	Thermal conductivity of HTF (W/mK)	0.6

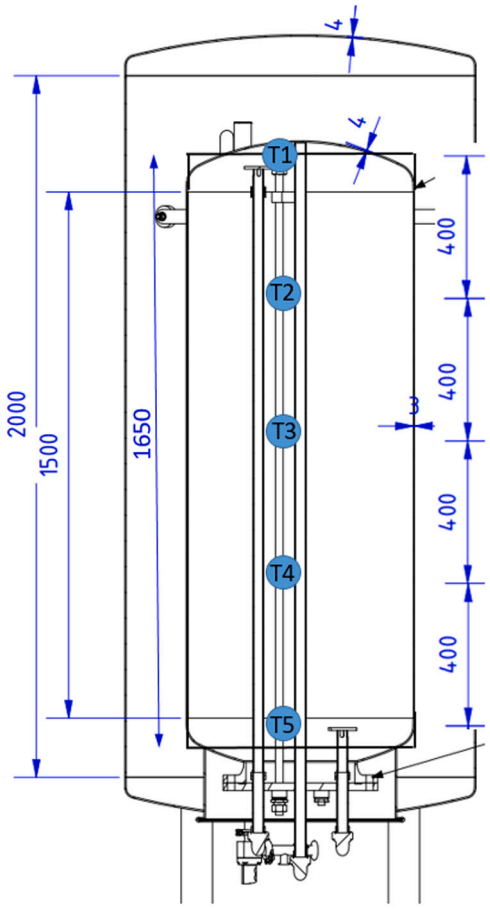

Fig. 8. Sketch of stratified water tank [42] used in the experiments for model validation and location of sensors.

obtained.

$$u(\dot{Q}) = \left[\left[\frac{\partial \dot{Q}}{\partial \rho}u(\rho)\right]^2 + \left[\frac{\partial \dot{Q}}{\partial \dot{V}}u(\dot{V})\right]^2 + \left[\frac{\partial \dot{Q}}{\partial Cp}u(Cp)\right]^2 + \left[\frac{\partial \dot{Q}}{\partial \Delta T}u(\Delta T)\right]^2\right]^{0.5} \quad (7)$$

where u(ρ) is the uncertainty of the density of the HTF, u($\dot{V}$) is the uncertainty of the volumetric mass flow, u(Cp) is the uncertainty of the specific heat capacity and u(ΔT) is the uncertainty of the temperature measurements.

3.2.5. Additional physical models considered

The physical model type 122 presented in the Documentation of TRNSYS 18 [48] was used to simulate the thermal performance of the back-up gas boiler. To calculate the solar diffuse irradiation on the tilted surface, required to calculate the tilted global irradiation, the physical model Reindl Model [49–51] was used.

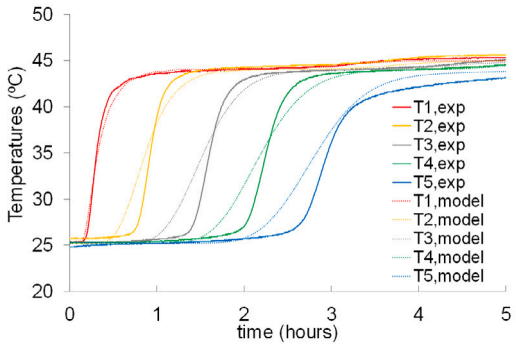

Fig. 9. Comparison of nodes temperatures of water tank: experiment vs. simulations with 66 nodes.

3.3. Simulation of the system

To simulate the system thermal performance, the connection between all the subcomponents was done in Python 3. To avoid calculations based on iterative numerical methods, which are highly time consuming, some variables of the subcomponents for the previous time-step [*t-1*] were used to calculate the variable for the current time-step [*t*]. These variables were: the inlet temperature of the solar field, the temperature of the PCM storage tank, the nodes temperature of the stratified water tank and the temperature of the sorbent material in each module of the sorption storage tank. Despite the fact that iterative processes were ideally avoided, the Gauss–Seidel method – considering a relaxing factor of 0.9 and a maximum error of 0.01 °C (for temperature) or 0.01 kg/h (for mass flow rate) – was required for the calculation of some system variables.

A time-step of 15 min was used for both, the control and the performance simulation of the system.

The simulation of the system was carried out using the numerical models explained in detail in Section 3.2. The evacuated tube collector AKOTEC OEM Vario 3000-30 [52] with an aperture area of 4.46 m^2 was used for the simulations. The thermal, optical, and operational parameters of the solar field are shown in Table 2. The energy coming either from the solar field or from the seasonal STES, was stored in a stratified water tank of 1 m^3 of volume. Unlike the rest of the simulation, the water tank was simulated with an internal sub time-step of 1 min to avoid that the high inflow relative to the volume of the node would generate errors in the energy balance. Three out of the five sensors located in the stratified tank were used to control the system: top (T_{top} = T1), middle (T_{middle} = T3) and bottom (T_{top} = T5) sensors. The thermal and physical parameters considered for the water tank are shown in Table 1.

The PCM storage tank, used in the simulations as low temperature heat source for the evaporator, contained 220 kg of the PCM called PCMP S15 [26]. This PCM was selected because its melting temperature (15 °C) matched with the nominal inlet temperature to the evaporator. The thermal and physical properties of the PCM tank are presented in Table 3. More details about the PCM storage tank can be found in Crespo et al. [38].

The sorption storage tank contained 20 modules of 100 kg, each of them was composed by an adsorber/desorber and an evaporator/condenser. During summer, the operation of the sorption tank was

Table 2
Properties of solar collector (related to aperture area) [52].

Parameter	Value	Parameter	Value
Total area of collector field (m^2)	17.5	Inclination of collectors	35°
a0: optical efficiency	0.559 [53]	Diffuse incidence angle modifier	1.314 [53]
a1: first order efficiency (W/m^2 K)	1.485 [53]	Maximum pressure (bar)	10 [52]
a2: second order efficiency (W/m^2 K)	0.002 [53]	Stagnation temperature (°C)	158 [52]
mass flow range (kg/h)	300–1000	solar HEX effectiveness	0.6
Heat transfer fluid	Water-glycol	Specific heat (kJ/kgK)	3.9

Table 3
Thermal and physical properties of PCM storage.

Parameter	Value	Parameter	Value
Total PCM mass (kg)	220	Type of slab	PCMP FlatICE [26]
Number of slabs	33	Slab dimension	0.5 m × 0.25 m × 0.35 m
Melting temperature (°C)	15 [26]	Latent heat (kJ/kg)	71.5 [38]
PCM density (kg/m^3)	1750 [38]	Heat transfer fluid	pure water

as follows: once the first active module has been charged, the outlet water still has high enthalpy which can provided (see Fig. 1) in the form of sensible heat to the next module if connected in series. This operational mode on the STES charging process has two advantages: first. overheating in the solar loop is avoided; second, next active module can be heated-up and reach the desorption temperature, so, it can then be ready for the charging process. The charging efficiency of a sorption module directly depends on the ambient temperature, since this latter corresponds to the inlet condenser temperature.

During winter just one module could be discharged at once. In winter season, it was likely that although the STES was charged and there was high heating demand, the STES system was not able to heat up the feed water. This can happen when the adsorption temperature or the inlet temperature to the adsorber were not high enough to heat up the feed water up to the space heating temperature. For this reason, a minimum sorption module temperature of 35 °C and a minimum feed water temperature to the reactor of 25 °C - which is supplied by the middle part of the water tank — were considered to allow the discharge of the STES. Thus, the close mode loop of space heating was activated just when the temperature in the bottom part of the tank was below 20 °C.

Finally, for the simulation of the boiler, a maximum boiler capacity of 9 kW and a boiler efficiency of 0.9 were considered.

3.4. Optimization of rule based control policy

As already mentioned, the STES system under study was charged in summer, when solar irradiation was high, and it was discharged in winter, when solar irradiation was low and a high space heating demand existed. To control the different components of the system, a RBC strategy, which is shown in Annex, selected the suitable operational mode based on the solar irradiation and the season. The RBC strategy was divided in two parts: a first for summer and a second for winter. Months from April to September were considered as summer period and October to March were considered as winter season. Four solar irradiation thresholds were used to define the control strategy of the system:

1 $E_{G,STES}$: minimum value to charge the sorption storage tank.
2 $E_{G,wt,s}$: minimum value to charge the water tank in summer.
3 $E_{G,wt,w}$: minimum value to charge the water tank in winter.
4 $E_{G,PCM}$: minimum value to charge the PCM tank.

The state of charge (SoC) of the sorption storage tank and PCM tank were necessary to perform the control of the system. The SoC of both storage systems were calculated based on an energy balance. Furthermore, the following parameters were required to define the RBC strategy:

1. $T_{DHW,set}$: DHW setpoint temperature (65 °C).
2. $T_{SH,set}$: SH setpoint temperature (38 °C).
3. $T_{SH,cl}$: setpoint temperature to activate SH close loop mode (20 °C).
4. $SoC_{PCM,dis}$: minimum state of charge of the PCM tank to allow its discharge (15%).
5. $T_{wt,max}$: maximum temperature in water tank (75 °C).
6. $T_{wt,set}$: setpoint temperature at the top of the water tank (70 °C).

The control of the system under study presented complexity due the high number of operational modes and to the limitations of the sorption storage tank, which could operate only under certain conditions which depended of the weather conditions and the status of the other sub-components. To decide, for example, weather solar energy in winter is used to discharge the sorption tank (charging the low temperature heat source) or to charge the water tank has an impact in the fossil fuel consumption of the system. Therefore, an optimization of the system RBC policy was performed.

Two different optimization scenarios were analyzed. The first optimization scenario consisted of minimizing the total annual operational costs (C_{total}) of the system (minCosts scenario). The total annual cost is a cumulative reward, which consists of the sum, for every time step of the year, of natural gas consumption of the boiler, the electrical consumption of the pumps, and an economical penalty in case that demand was not covered. The definition of total annual cost is presented in Eq. (8).

$$C_{total} = \sum_{t=0}^{J} \left[PF \cdot (E_{nosup,dhw} + E_{nosup,sh}) + C_{gas} \cdot E_b + C_{el,pump} \cdot E_{pumps} \right] \tag{8}$$

As mentioned in Section 2, in winter, when DWH and SH demands were required simultaneously and the SH demand cannot supply directly from the water tank, the back-up boiler was used just to supply DHW demand. Hence, during some time-steps may happen that SH demand was not supplied. To minimize this effect, the total annual cost included a penalty factor (PF). The system paid an economic penalty when the SH demand was not supplied in order to prevent as much as possible the optimizer to fall into scenarios where the SH demand was not satisfied. The system was optimized for a penalty factor of 1 time the gas price, using a unitary cost for the natural gas (C_{gas}) of 61.5 €/MWh (with taxes). The electrical pump energy consumption was calculated based on the number of active pumps at every time-step [t]. A constant pump power consumption of 0.01 kW and a electricity unitary cost ($C_{el,pump}$) of 298 €/MWh (with taxes) [54] was considered to calculate the electrical pump cost.

The second optimization scenario consisted of reaching a trade-off between minimum operational cost and maximum use of the STES

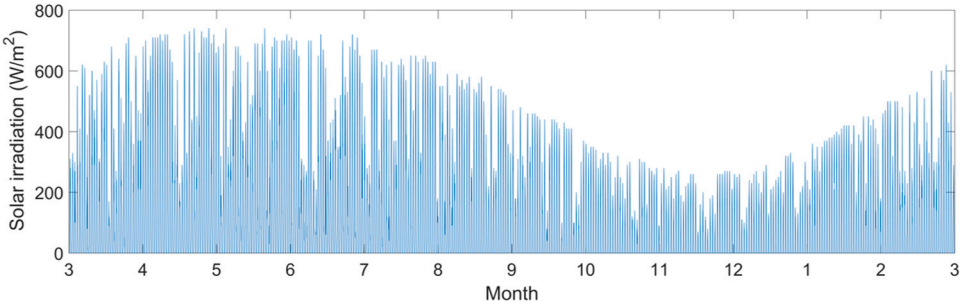

Fig. 10. Solar global irradiation on collector along the year 2008.

Table 4
Optimized control thresholds for the studied scenarios.

Scenario name	$E_{G,STES}$ [W/m^2]	$E_{G,wt,s}$ [W/m^2]	$E_{G,wt,w}$ [W/m^2]	$E_{G,pcm}$ [W/m^2]
minCosts_FP1	467	128	139	101
maxSTES_FP1	426	121	140	101

Table 5
STES performance and costs for the studied scenarios.

Scenario name	$SoC_{STES,s}$ [%]	$SoC_{STES,w}$ [%]	C_{total} [€]
minCosts_FP1	89.6	1.9	441.7
maxSTES_FP1	98.9	1.9	442.2

system (maxSTES scenario). Hence, the objective function was:

$$C_{max,STES} = C_{total} \cdot [1 - (SoC_{STES,endsummer} - SoC_{STES,endwinter})] \quad (9)$$

The solar irradiation thresholds are key factors in the operation of the system. Therefore, the four solar irradiation thresholds, presented in the RBC policy, were selected as optimization variables. The optimization search space in W/m^2 for every control threshold was: $E_{G,STES}$: 300–600; $E_{G,wt,s}$:100–600; $E_{G,wt,w}$:100–500 and $E_{G,pcm}$:100–300.

Hyperopt library [55] was considered for the optimization, it uses different stochastic search algorithms to find the best scalar value into a space. In this study, the Tree-structured Parzen Estimators (TPE) algorithm [56] was chosen. The hyperparametric optimization was stopped at 300 iterations since no further improvements in the results were expected. Within the TPE algorithm, a sample of 100 candidates was set, and the first 20 iterations were considered randomly. Gamma value of 20% was used, which means that 20% of the best observations are used to estimate the next set of parameters.

To avoid oversampling, input data (weather data and thermal demand) of the years 2010, 2011 and 2012 was used for the optimization. To validate the optimization results, the simulation was carried out with data from 2008. Hence, the results of the thermal performance of the system presented in this study have been obtained with data from 2008. The solar irradiation for 2008 is presented in Fig. 10.

Once the control strategy was optimized, several performance indicators were used to assess the thermal performance of the system and the sorption storage tank. The performance indicators were: solar fraction (SF), COP of STES, sensible energy required by the reactor during desorption ($E_{des,sen}$), effective desorbed energy (E_{des}), effective adsorbed energy output(E_{ads}), energy from collector (E_{coll}), energy from boiler (E_b) and energy density (e_d) of the sorption storage tank. The energy density was calculated was on the adsorbent composites volume. To assess the environmental impact of the system, CO_2 savings were also calculated. Some of the indicators are defined in (10), (11) and (12).

$$SF = \frac{(D_{DHW} + D_{SH}) - E_b}{D_{DHW} + D_{SH}} \quad (10)$$

$$COP_{stes} = \frac{E_{ads}}{E_{des,sen} + E_{des}} \quad (11)$$

$$e_d = \frac{E_{ads}}{V_{STES}} \quad (12)$$

4. Results and discussion

4.1. Analysis of the overall performance of the system

In the following section, annual results of the system optimized scenarios are presented. As already mentioned, the solar driven seasonal system was optimized for two different objective functions considering a 165 m^2 building located in Nuremberg. The total thermal demand obtained for the year 2008 was 8904 kWh.

The question whether solar energy should be stored directly in the water tank, in the STES or in the low temperature heat source is a key decision. In Table 4, the results of the four optimized control thresholds for the annual simulations are presented. The irradiation control threshold $E_{G,STES}$ (467 W/m^2) of scenario minCost, which searched to minimize the operational costs, allowed to have more solar hours available to charge the water tank rather than the STES (see RBC strategy in Annex) in comparison with the scenario maxSTES (426 W/m^2), which searched for a trade-off between costs minimization and maximization use of the STES. As a consequence of these control thresholds, the STES was charged to a maximum of 89.6% and 98.9% for scenarios minCost and maxSTES, respectively. Moreover, as shown in Table 5 the system was completely discharged at the end of winter in both cases. Therefore, the results indicated that it was more cost-effective (441.7 € and 442.2 €) not to use the whole capacity of the sorption tank and during some periods of the year use the solar heat to directly charge the water tank. Nevertheless, from an quantitative perspective, the difference in annual cost between the minCosts and maxSTES scenario can be neglected, as observed in Fig. 11. Indeed, these results show that both scenarios reached the same total annual cost, but, optimizing the system control based on operational costs would allow to reduce the size of the STES system in around 10%, which means lower investment costs.

In addition to obtain nearly equal total annual cost, both scenarios also obtained the same solar fraction and CO_2 savings, presenting values of 35% and 623 kg of CO_2 respectively.

4.2. Performance of the sorption system

The concept of the system under study consisted of discharging the seasonal sorption system during heating season when solar heat was not available, to heat up the water tank to provide SH demand to the end user. High performance efficiency of the sorption storage system is reached when a continuous charge or discharge takes place, thus,

Table 6
Results for the different scenarios.

Scenario	E_b [kWh]	E_{coll} [kWh]	COP_{stes}	$E_{ch,sens}$ [kWh]	E_{des} [kWh]	E_{ads} [kWh]	SF [%]	e_d [kWh/m^3]	$CO_{2,sav}$ [kg]
minCost_FP1	6156.8	6075.4	0.26	692.7	547.8	325.5	34.9	90.4	623.3
maxSTES_FP1	6124.6	6065.2	0.28	690.9	599.2	364.7	35.0	106.3	623.4

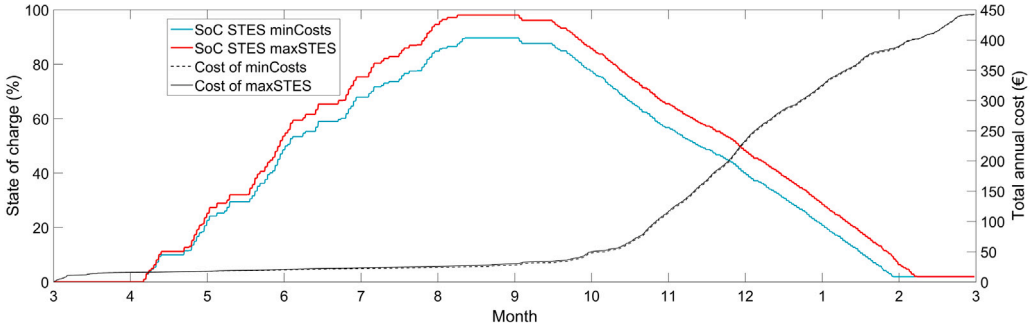

Fig. 11. Evolution of the state of charge of the STES vs. cumulative total annual costs for minCosts and maxSTES scenarios.

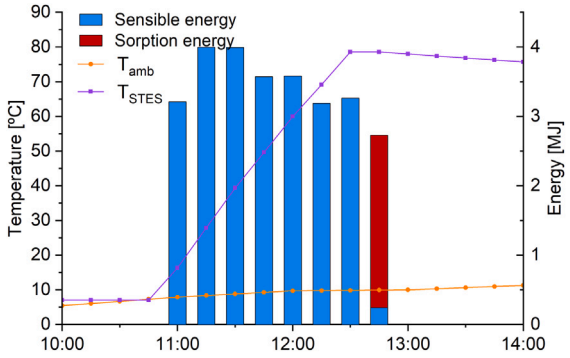

Fig. 12. Charging process of the system for the scenario that minimized the costs during a reference summer day.

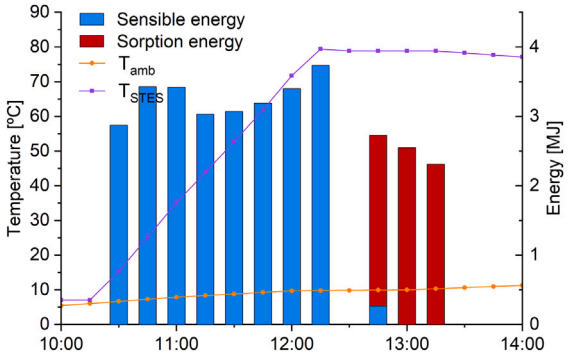

Fig. 13. Charging process of the system for the scenario that maximized the STES use during a reference summer day.

repetitive warming-ups of the sorbent material can be avoided. During winter, due to the variability of the weather conditions, the availability of the low temperature heat source and the possibility of using solar heat to charge directly the water tank made impossible to perform a continuous discharge of the STES. Indeed, during some days with very low solar irradiation, the discharge of the STES could not be performed due to the unavailability of the low temperature heat source, which must be charged with solar energy. In those cases, the discharge of the STES was stopped, at least, until solar irradiation could charge again the low temperature heat source. As previously mentioned, this effect entails that due to a waiting period between two discharges of the STES; the sorbent material needed to be heated up again to adsorption temperature. This drawback causes an efficiency drop of the STES during winter, but also in summer during the charging phase. Furthermore, it is worth to mention that the inlet temperature to the sorption modules coming from the water tank must be at least 25 °C to obtain hot water leaving the STES modules at temperatures useful for the SH application. This fact implied, that if the medium part of the stratified water tank was below 25 °C, the thermal energy stored in the STES could not be exploited.

Nevertheless, despite the operating limitations of the STES, the charges and discharges of the STES system were carried out continuously enough to make cost-effective the use of the STES. In Fig. 14, the propagation of the state of charge vs. ambient temperature along the year for scenario minCosts is shown. The periods where the degree of desorption propagated faster matched with high ambient temperatures and high solar irradiation that allowed to reach the desorption temperature (90 °C).

In Table 6, the results of the thermal performance of the sorption system are presented. The sorption modules of minCost scenario desorbed 548 kWh, for which 692 kWh of sensible heat coming from the sun were necessary. Out of the 548 kWh desorbed, 325 kWh were discharged to the water tank. With respect to maxSTES scenario, the sorption modules desorbed 599 kWh of energy, for which 691 kWh of sensible heat were necessary. Out of the 599 kWh desorbed, 365 kWh were discharged. These values showed that the STES efficiency (measured COP based) is slightly higher for the maxSTES scenario (0.28 vs. 0.26). This deviation in COP can be explained by looking at Figs. 12 and 13, which depict the weather conditions, STES temperature and energy delivered to the sorption storage during a charging process in a summer day, for both optimal case scenarios: costs minimization and STES use maximization. Assuming the same reference summer day, for the scenario which maximized the STES use, the heat of sorption versus the required sensible heat to reach the regeneration temperature was higher compared to the scenario that minimized the costs. This can be explained as follows: the optimal threshold $E_{G,STES}$ was lower for the maxSTES scenario (426 W/m^2) compared to the minCosts scenario (467 W/m^2). This fact allowed to charge the STES with solar heat at lower solar irradiations and therefore during longer time (from 10:30 to 13:15), which caused a more continuous charge. Thus, the COP for the maxSTES scenario was slightly higher compared to the minCosts

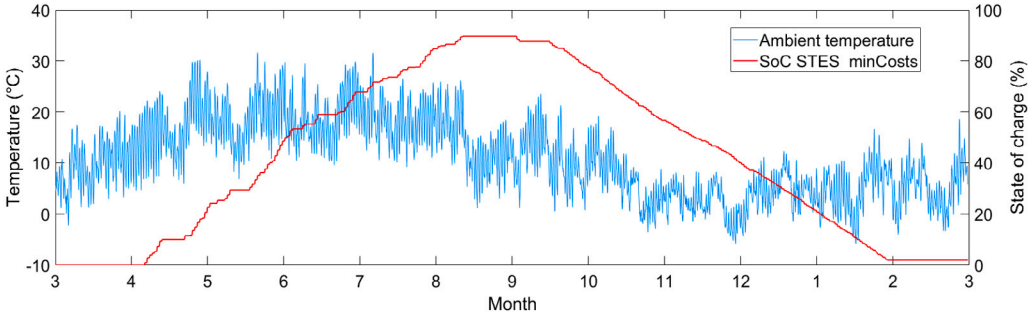

Fig. 14. Evolution of the state of charge of the STES vs. ambient temperature.

Table 7
IDs of the operational modes.

ID	Action description	ID	Action description
Coll_STES	Charge sorption modules with solar heat	DHW_tank	Supply DHW from water tank
Coll_DHW	Charge water tank for DHW with solar heat	DHW_boiler	Supply DHW using back-up boiler
Coll_SH	Charge water tank for SH with solar heat	SH_tank	Supply SH directly from water tank
Coll_PCM	Charge PCM tank with solar heat	SH_boiler	Supply SH using back-up boiler
Dis_STES	Discharge sorption module to water tank	SH_closeloop	Supply SH in close loop

scenario. In the system under study, slightly higher STES efficiency of maxSTES scenario was not justified since, as mentioned, the same total annual cost using lower STES size could be achieved for the minCost scenario. The little difference in total annual cost between both scenarios is, in fact, due to a slightly higher pump costs - one extra pump must be used to discharge the STES - and the penalty cost (0.1 €).

The energy density of the optimum minCost and maxSTES scenarios was respectively 90.4 and 101.3 kWh/m^3, which is around half of the value of the energy density at material level reported in [21]. Such a discrepancy is due to the sensible losses encountered in the stand-by periods and the limitation of the total capacity use due to economic reasons for the minCost scenario. As expected, the energy density of maxSTES scenario was higher, nevertheless, the optimal economic scenario profit a large portion of the STES capacity.

5. Conclusions

A solar heating system based on a seasonal sorption TES was designed to deliver SH to a low demand single family house in middle Europe. Additionally, the solar field could deliver DHW through a short-term water tank. The control of the heating system is essential to ensure good overall thermal performance and to make competitive the sorption heat storage technology. Hence, in this paper, the RBC strategy of the system was optimized based on operational cost for two objective functions, based on weather conditions, system states, and thermal demand. Validated physical models and performance maps were used to simulate the main subcomponents of the system.

The system, composed by 17.5 m^2 of solar collectors, 3.6 m^3 of a novel composite water sorbent material based on lithium-chloride and 1 m^3 of a stratified water tank, obtained an energy density of the sorption system of 90.4 kWh/m^3 and a solar fraction of 35% for the optimal economic scenario.

The optimal economic scenario exploited just 87.7% of the seasonal sorption system. Indeed, the results showed that the size of the sorption storage system could be reduced in around 10% obtaining optimal operational annual costs. Thus, reducing the overall investment costs, would contribute to make the sorption technology more competitive against other TES systems.

Table 8
Operational modes of the system.

Nº of operational mode	Description of the operational mode
0	No action
1	Coll_STES
2	Coll_STES + DHW_tank
3	Coll_STES + DHW_boiler
4	Coll_DHW
5	Coll_DHW + DHW_tank
6	Coll_DHW + DHW_boiler
7	Coll_SH
8	Coll_SH + DHW_tank
9	Coll_SH + DHW_boiler
10	Dis_STES
11	DHW_tank
12	DHW_boiler
13	Dis_STES + DHW_tank
14	Dis_STES + DHW_boiler
15	Coll_DHW + SH_tank
16	Coll_SH + SH_tank
17	SH_tank
18	Coll_DHW + SH_boiler
19	Coll_SH + SH_boiler
20	SH_boiler
21	Dis_STES + SH_boiler
22	SH_closeloop
23	Coll_DHW + SH_closeloop
24	Coll_SH + SH_closeloop
25	Dis_STES + SH_closeloop
26	Coll_PCM
27	Coll_PCM + Dis_STES
28	Coll_PCM + DHW_tank
29	Coll_PCM + Dis_STES + DHW_tank
30	Coll_PCM + DHW_boiler
31	Coll_PCM + Dis_STES + DHW_boiler
32	Coll_PCM + SH_tank
33	Coll_PCM + SH_boiler
34	Coll_PCM + Dis_STES + SH_boiler
35	Coll_PCM + SH_closeloop
36	Coll_PCM + Dis_STES + SH_closeloop
37	Coll_DHW + DHW_boiler + SH_tank
38	Coll_SH + DHW_boiler + SH_tank
39	DHW_boiler + SH_tank
40	Coll_PCM + DHW_boiler + SH_tank

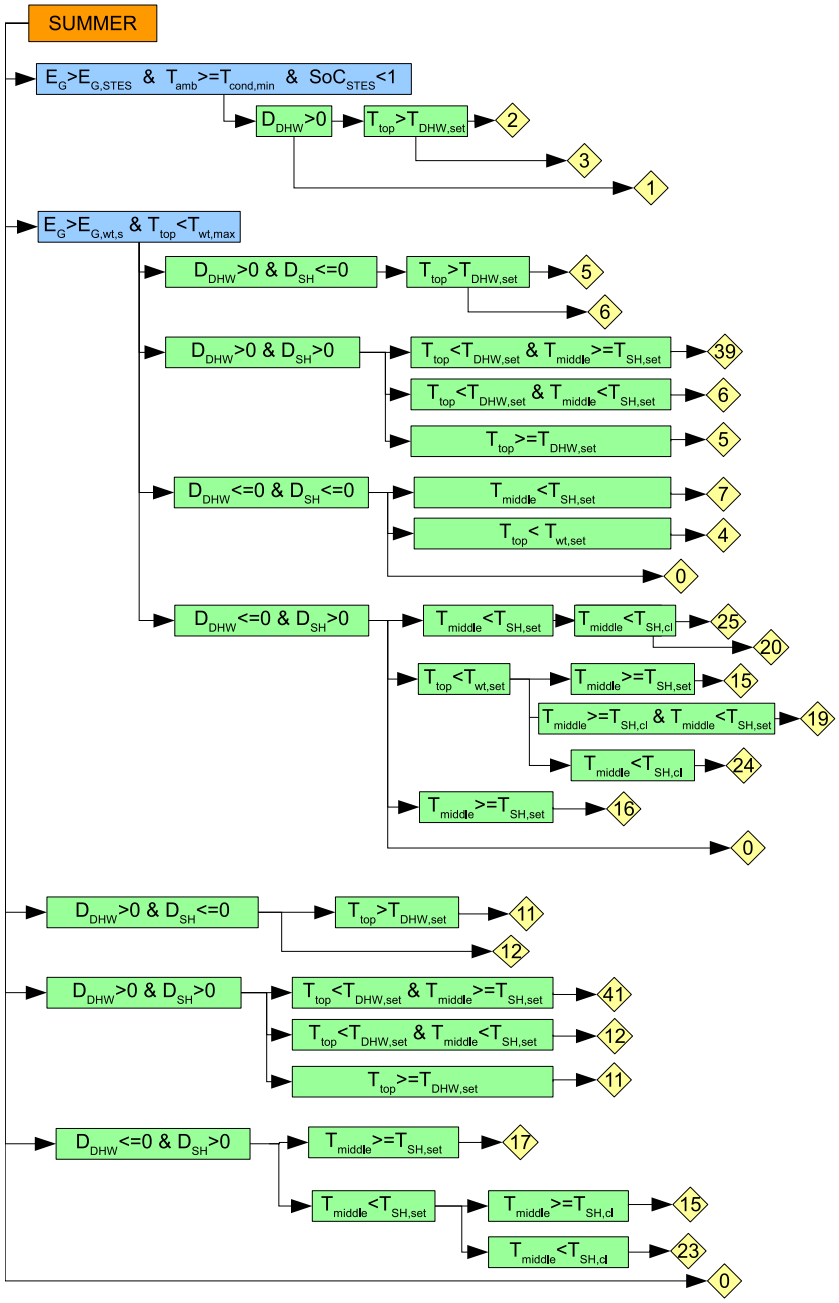

Fig. 15. RBC strategy for summer.

The efficiency of a sorption system highly depends on the availability on the low temperature heat source to provide heat to the evaporator. In this study, the evaporator of the sorption modules was assisted by a low temperature heat source (PCM tank) charged by the solar field. The low temperature heat source allowed to discharge the STES showing independence from ambient temperature specially during cold winter days. Further research on optimizing the temperature supply to the evaporator may be performed.

This study proved that the control optimization of a heating energy system with seasonal sorption storage is essential to maximize its performance, define the optimal size of the sorption storage tank, and thus make the technology economically competitive against traditional fossil fuels systems.

A main drawback of a sorption storage system is the energy lost during the warming up of the modules during two interrupted charges or discharges. Control strategies based on artificial intelligent could help to overcome this issue.

Declaration of competing interest

The authors declare that they have no known competing financial interests or personal relationships that could have appeared to influence the work reported in this paper.

Data availability

Data will be made available on request.

Acknowledgments

This project was funded by the European Union's Horizon 2020 Research and Innovation Programme under grant agreement No. 764025 (SWS-HEATING). This work was partially funded by the Ministerio de Ciencia, Innovación *y* Universidades de España, Spain (RTI2018-093849-B-C31–MCIU/AEI/FEDER, UE) and by the Ministerio de Ciencia, Innovación *y* Universidades–Agencia Estatal de Investigación (AEI) (RED2018-102431-T). The authors would like to thank the Catalan Government for the quality accreditation given to their research group (2017 SGR 1537). GREiA is certified agent TECNIO in the category of technology developers from the Government of Catalonia. This work is partially supported by ICREA under the ICREA Academia programme. Alicia Crespo would also like to acknowledge the financial support of the FI-SDUR grant from the AGAUR of the Generalitat de Catalunya and Secretaria d'Universitats i Recerca del Departament d'Empresa i Coneixement de la Generalitat de Catalunya.

Annex I

A.1. Operational modes of the system

In Table 7 the IDs of the operational modes of the system subcomponents are presented, along with a brief description of each of them. In Table 8 the system operational modes, which a combination of the system subcomponents operational modes are presented. These operational modes were already described in Section 2: Description of the system.

A.2. Rule based control strategy

The RBC control strategy for summer and winter is shown in Figs. 15–17 respectively.

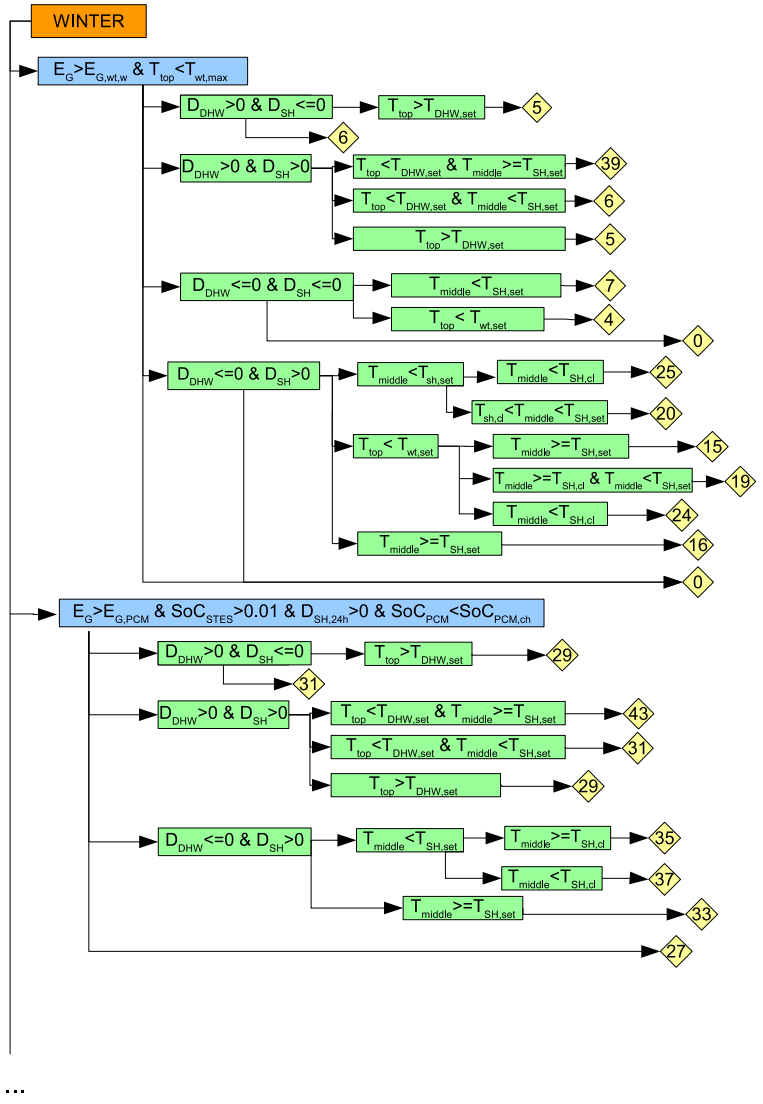

Fig. 16. RBC strategy for summer.

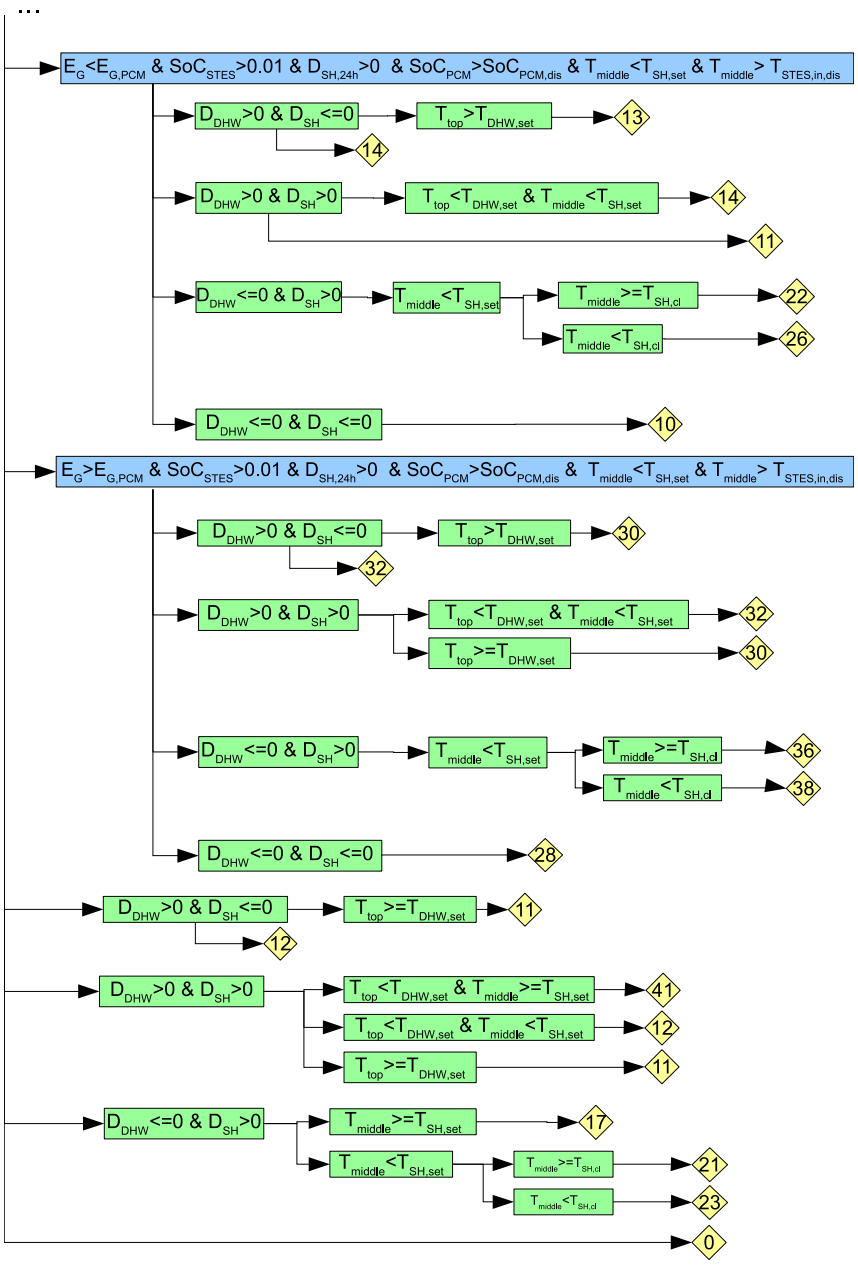

Fig. 17. RBC strategy for summer.

References

[1] REN21. REN21,2020. Renewables 2020 global status report (GSR). 2020, [Online], accessed: 2021-01-16. URL https://www.ren21.net/gsr-2020/chapters/chapter_01/chapter_01/#sub_3.

[2] eurostat. Energy consumption in the residential sector by use, EU-27. 2018, [Online], accessed: 2021-01-16. URL https://ec.europa.eu/eurostat/statistics-explained/index.php.

[3] Li T, Wang R, Kiplagat JK, Kang Y. Performance analysis of an integrated energy storage and energy upgrade thermochemical solid–gas sorption system for seasonal storage of solar thermal energy. Energy 2013;50:454–67. http://dx.doi.org/10.1016/j.energy.2012.11.043, URL https://www.sciencedirect.com/science/article/pii/S0360544212009073.

[4] van Alebeek R, Scapino L, Beving M, Gaeini M, Rindt C, Zondag H. Investigation of a household-scale open sorption energy storage system based on the zeolite 13x/water reacting pair. Appl Therm Eng 2018;139:325–33. http://dx.doi.org/10.1016/j.applthermaleng.2018.04.092, URL https://www.sciencedirect.com/science/article/pii/S1359431117370436.

[5] Gaeini M, van Alebeek R, Scapino L, Zondag H, Rindt C. Hot tap water production by a 4 kW sorption segmented reactor in household scale for seasonal heat storage. J Energy Storage 2018;17:118–28. http://dx.doi.org/10.1016/j.est.2018.02.014, URL https://www.sciencedirect.com/science/article/pii/S2352152X1730405X.

[6] Gaeini M, Javed M, Ouwerkerk H, Zondag H, Rindt C. Realization of a 4kW thermochemical segmented reactor in household scale for seasonal heat storage. Energy Procedia 2017;135:105–14. http://dx.doi.org/10.1016/j.egypro.2017.09.491, 11th International Renewable Energy Storage Conference, IRES 2017, 14-16 March 2017, Düsseldorf, Germany. URL https://www.sciencedirect.com/science/article/pii/S1876610217345940.

[7] Köll R, van Helden W, Engel G, Wagner W, Dang B, Jänchen J, Kerskes H, Badenhop T, Herzog T. An experimental investigation of a realistic-scale seasonal solar adsorption storage system for buildings. Sol Energy 2017;155:388–97. http://dx.doi.org/10.1016/j.solener.2017.06.043, URL https://www.sciencedirect.com/science/article/pii/S0038092X17305509.

[8] Weber R, Asenbeck S, Kerskes H, Drück H. SolSpaces – Testing and performance analysis of a segmented sorption store for solar thermal space heating. Energy Procedia 2016;91:250–8. http://dx.doi.org/10.1016/j.egypro.2016.06.214.

[9] Engel G, Asenbeck S, Köll R, Kerskes H, Wagner W, van Helden W. Simulation of a seasonal, solar-driven sorption storage heating system. J Energy Storage 2017;13:40–7. http://dx.doi.org/10.1016/j.est.2017.06.001, URL https://www.sciencedirect.com/science/article/pii/S2352152X17300646.

[10] Ma Z, Bao H, Roskilly AP. Seasonal solar thermal energy storage using thermochemical sorption in domestic dwellings in the UK. Energy

2019;166:213–22. http://dx.doi.org/10.1016/j.energy.2018.10.066, URL https://www.sciencedirect.com/science/article/pii/S0360544218320565.

[11] Tzinnis E, Baldini L. Combining sorption storage and electric heat pumps to foster integration of solar in buildings. Appl Energy 2021;301:117455. http://dx.doi.org/10.1016/j.apenergy.2021.117455, URL https://www.sciencedirect.com/science/article/pii/S030626192100845X.

[12] Mlakar U, Stropnik R, Koželj R, Medved S, Stritih U. Experimental and numerical analysis of seasonal solar-energy storage in buildings. Int J Energy Res 2019;43(12):6409–18. http://dx.doi.org/10.1002/er.4449, Cited by: 5. URL https://www.scopus.com/inward/record.uri?eid=2-s2.0-85063495029&doi=10.1002%2fer.4449&partnerID=40&md5=a154cf7245e74ef60219a410bcb16cd6.

[13] Thinsurat K, Bao H, Ma Z, Roskilly AP. Performance study of solar photovoltaic-thermal collector for domestic hot water use and thermochemical sorption seasonal storage. Energy Convers Manage 2019;180:1068–84. http://dx.doi.org/10.1016/j.enconman.2018.11.049, Cited by: 22; All Open Access, Green Open Access. URL https://www.scopus.com/inward/record.uri?eid=2-s2.0-85057150130&doi=10.1016%2fj.enconman.2018.11.049&partnerID=40&md5=8decb51ed0f189342a6360c784928f57.

[14] Ma Z, Bao H, Roskilly AP. Electricity-assisted thermochemical sorption system for seasonal solar energy storage. Energy Convers Manage 2020;209:112659. http://dx.doi.org/10.1016/j.enconman.2020.112659, URL https://www.sciencedirect.com/science/article/pii/S0196890420301977.

[15] Jiang L, Liu W, Lin Y, Wang R, Zhang X, Hu M. Hybrid thermochemical sorption seasonal storage for ultra-low temperature solar energy utilization. Energy 2022;239:122068. http://dx.doi.org/10.1016/j.energy.2021.122068, URL https://www.sciencedirect.com/science/article/pii/S0360544221023161.

[16] Jiang L, Li S, Wang R, Fan Y, Zhang X, Roskilly A. Performance analysis on a hybrid compression-assisted sorption thermal battery for seasonal heat storage in severe cold region. Renew Energy 2021;180:398–409. http://dx.doi.org/10.1016/j.renene.2021.08.101, URL https://www.sciencedirect.com/science/article/pii/S0960148121012696.

[17] Scapino L, De Servi C, Zondag H, Diriken J, Rindt C, Sciacovelli A. Techno-economic optimization of an energy system with sorption thermal energy storage in different energy markets. Appl Energy 2019;258C. http://dx.doi.org/10.1016/j.apenergy.2019.114063.

[18] Bau U, Hoseinpoori P, Graf S, Schreiber H, Lanzerath F, Kirches C, Bardow A. Dynamic optimisation of adsorber-bed designs ensuring optimal control. Appl Therm Eng 2017;125:1565–76. http://dx.doi.org/10.1016/j.applthermaleng.2017.07.073, URL https://www.sciencedirect.com/science/article/pii/S1359431117345349.

[19] Frazzica A, Brancato V, Dawoud B. Unified methodology to identify the potential application of seasonal sorption storage technology. Energies 2020;13(5). http://dx.doi.org/10.3390/en13051037, URL https://www.mdpi.com/1996-1073/13/5/1037.

[20] N'Tsoukpoe K, Kuznik F. A reality check on long-term thermochemical heat storage for household applications. Renew Sustain Energy Rev 2021;139:110683. http://dx.doi.org/10.1016/j.rser.2020.110683.

[21] Frazzica A, Brancato V, Caprì A, Cannilla C, Gordeeva L, Aristov Y. Development of "salt in porous matrix" composites based on LiCl for sorption thermal energy storage. Energy 2020;208:118338. http://dx.doi.org/10.1016/j.energy.2020.118338, URL https://www.sciencedirect.com/science/article/pii/S0360544220314456.

[22] Mikhaeil M, Gaderer M, Dawoud B. On the development of an innovative adsorber plate heat exchanger for adsorption heat transformation processes; an experimental and numerical study. Energy 2020;207:118272. http://dx.doi.org/10.1016/j.energy.2020.118272, URL https://www.sciencedirect.com/science/article/pii/S0360544220313797.

[23] Jiang L, Wang R, Wang L, Roskilly T. Investigation on an innovative re-sorption system for seasonal thermal energy storage. Energy Convers Manage 2017;149:129–39. http://dx.doi.org/10.1016/j.enconman.2017.07.018.

[24] Li T, Wu S, Yan T, Wang R, Zhu J. Experimental investigation on a dual-mode thermochemical sorption energy storage system. Energy 2017;140:383–94. http://dx.doi.org/10.1016/j.energy.2017.08.073, URL https://www.sciencedirect.com/science/article/pii/S0360544217314494.

[25] Zisopoulos G, Nesiadis A, Atsonios K, Nikolopoulos N, Stitou D, Coca-Ortegón A. Conceptual design and dynamic simulation of an integrated solar driven thermal system with thermochemical energy storage for heating and cooling. J Energy Storage 2021;41:102870. http://dx.doi.org/10.1016/j.est.2021.102870, URL https://www.sciencedirect.com/science/article/pii/S2352152X21005922.

[26] PCM products. 2020, accessed: 2020-01-15. URL http://www.pcmproducts.net/.

[27] Guglielmetti R, Macumber D, Long N. Openstudio: An open source integrated analysis platform. In: Proceedings of the building simulation. Sydney, Australia; 2011, doi:Preprint NREL/CP-5500-51836.

[28] Crawley D, Lawrie L, Winkelmann F, Buhl W, Huang Y, Pedersen C, Strand R, Liesen R, D.E. Fisher MW, Glazer J. EnergyPlus: Creating a new-generation building energy simulation program. Energy Build 2001;33:319–31. http://dx.doi.org/10.1016/S0378-7788(00)00114-6.

[29] IEE project TABULA, Institut Wohnen und Umwelt GmbH (IWU) and partners. 2009-2012, accessed: 2021-04-18. URL https://episcope.eu/iee-project/tabula/.

[30] University of Perugia. D5.3 Dynamic user-building interaction model predicting thermal-energy behaviour. Tech. rep., 2019.

[31] Meteoblue AG. 2020, accessed: 2020-11-10. URL https://content.meteoblue.com/en.

[32] van Rossum G. Python tutorial. Tech. Rep. CS-R9526, Amsterdam: Centrum voor Wiskunde en Informatica (CWI); 1995.

[33] Duffie JA, Beckman WA. Solar engineering of thermal processes. 4th ed.. John Wiley & Sons, Inc; 2013, http://dx.doi.org/10.1002/9781118671603.

[34] Ayompe L, Duffy A, McCormack S, Conlon M. Validated TRNSYS model for forced circulation solar water heating systems with flat plate and heat pipe evacuated tube collectors. Appl Therm Eng 2011;31(8):1536–42. http://dx.doi.org/10.1016/j.applthermaleng.2011.01.046, URL https://www.sciencedirect.com/science/article/pii/S1359431111000718.

[35] Çengel Y. Heat transfer. A practical approach. 2nd ed.. McGraw-Hill; 2002.

[36] Brancato V, Frazzica A, Caprì A, Gordeeva L, Aristov Y, Mikhaeil M, Dawoud B. SWS composites based on LiCl for sorption thermal energy storage: thermochemical and kinetic properties. In: ENERSTOCK 2021. Ljubljana; 2021.

[37] Cengel YA, Ghajar AJ. Heat and mass transfer: Fundamentals and applications. 5th ed.. McGraw Hill; 2015.

[38] Crespo A, Zsembinszki G, Vérez D, Borri E, Fernández C, Cabeza LF, de Gracia A. Optimization of design variables of a phase change material storage tank and comparison of a 2D implicit vs. 2D explicit model. Energies 2021;14(9). http://dx.doi.org/10.3390/en14092605, URL https://www.mdpi.com/1996-1073/14/9/2605.

[39] Rahman A, Smith A, Fumo N. Performance modeling and parametric study of a stratified water thermal storage tank. Appl Therm Eng 2016;100. http://dx.doi.org/10.1016/j.applthermaleng.2016.01.163.

[40] Rodríguez-Hidalgo M, Rodríguez-Aumente P, Lecuona A, Legrand M, Ventas R. Domestic hot water consumption vs. solar thermal energy storage: The optimum size of the storage tank. Appl Energy 2012;97:897–906. http://dx.doi.org/10.1016/j.apenergy.2011.12.088, Energy Solutions for a Sustainable World - Proceedings of the Third International Conference on Applied Energy, May 16-18, 2011 - Perugia, Italy. URL https://www.sciencedirect.com/science/article/pii/S0306261911008944.

[41] Vérez D, Borri E, Crespo A, Zsembinszki G, Dawoud B, Cabeza LF. Experimental study of a small-size vacuum insulated water tank for building applications. Sustainability 2021;13(10). http://dx.doi.org/10.3390/su13105329, URL https://www.mdpi.com/2071-1050/13/10/5329.

[42] Sirch tankbau-tankservice speicherbau GmbH. 2021, accessed: 2021-09-14. URL https://pufferspeicher-sirch.de/start/.

[43] Joint Committee for Guides in Metrology (JCGM) Guide to the expression of uncertainty in measurement — Part 6: Developing and using measurement models. Tech. rep., 2020.

[44] Mselle BD, Zsembinszki G, Vérez D, Borri E, Cabeza LF. A detailed energy analysis of a novel evaporator with latent thermal energy storage ability. Appl Therm Eng 2022;201:117844. http://dx.doi.org/10.1016/j.applthermaleng.2021.117844, URL https://www.sciencedirect.com/science/article/pii/S1359431121012680.

[45] Wolf H. Determination of water density: limitations at the uncertainty level of 1x10-6. Accredit Qual Assur 2008;13:587–91. http://dx.doi.org/10.1007/s00769-008-0442-2.

[46] Rudtsch S. Uncertainty of heat capacity measurements with differential scanning calorimeters. Thermochim Acta 2002;382(1-2):17–25. http://dx.doi.org/10.1016/S0040-6031(01)00730-4.

[47] Vérez D, Borri E, Crespo A, Mselle BD, de Gracia Á, Zsembinszki G, Cabeza LF. Experimental study on two pcm macro-encapsulation designs in a thermal energy storage tank. Appl Sci (Switzerland) 2021;11(13). http://dx.doi.org/10.3390/app11136171, Cited by: 4; All Open Access, Gold Open Access, Green Open Access. URL https://www.scopus.com/inward/record.uri?eid=2-s2.0-85109928951&doi=10.3390%2fapp11136171&partnerID=40&md5=024d6e6c0822929fbf8c609f8662c7e8.

[48] Klein S, et al. TRNSYS18: A transient system simulation program, volume 4, mathematical reference. Tech. rep., USA: Solar Energy Laboratory, Univ.of Wisconsis-Madison; 2018, URL https://sel.me.wisc.edu/trnsys/features/trnsys18_0_updates.pdf.

[49] Reindl D, Beckman W, Duffie J. Diffuse fraction correlations. Sol Energy 1990;45(1):1–7. http://dx.doi.org/10.1016/0038-092X(90)90060-P, URL https://www.sciencedirect.com/science/article/pii/0038092X9090060P.

[50] Reindl D, Beckman W, Duffie J. Evaluation of hourly tilted surface radiation models. Sol Energy 1990;45(1):9–17. http://dx.doi.org/10.1016/0038-092X(90)90061-G, URL https://www.sciencedirect.com/science/article/pii/0038092X9090061G.

[51] Loutzenhiser P, Manz H, Felsmann C, Strachan P, Frank T, Maxwell G. Empirical validation of models to compute solar irradiance on inclined surfaces for building energy simulation. Sol Energy 2007;81(2):254–67. http://dx.doi.org/10.1016/j.solener.2006.03.009, URL https://www.sciencedirect.com/science/article/pii/S0038092X06000879.

[52] Solar KEYMARK certificate - Licence number: 011-7S660R of the collector OEM vario 3000-30 hp of akotec produktionsgesellschaft GmbH. Tech. rep., TÜVRheinland; 2013.
[53] University of Lleida, National Technical University of Athens, Istituto di Tecnologie Avanzate per l'Energia. D5.1 Optimised system control and strategies. Tech. rep., 2020.
[54] Monitoring report 2017 - key findings. Tech. rep., Bundesnetzagentur, Bundeskartellamt; 2017, URL https://www.bundesnetzagentur.de/.
[55] Bergstra J, Yamins D, Cox D. Making a science of model search: Hyperparameter optimization in hundreds of dimensions for vision architectures. In: Proceedings of the 30th international conference on machine learning, ICML. 2013, (PART1), Atlanta, GA, USA. 2013, p. 115–223.
[56] Shevchuk Y. NeuPy, neural networks in Python. 2016, [Online], accessed: 2021-02-02. URL http://neupy.com/2016/12/17/hyperparameter_optimization_for_neural_networks.html#tree-structured-parzen-estimators-tpe.